Proc. 29th Int. Workshop on Vertex Detectors (VERTEX2020)
JPS Conf. Proc. **34**, 010003 (2021)
https://doi.org/10.7566/JPSCP.34.010003

The Belle II Silicon Vertex Detector: Performance and Operational Experience in the First Year of Data Taking

G. Rizzo[13,14], K. Adamczyk[22], H. Aihara[19], T. Aziz[12], S. Bacher[22], S. Bahinipati[8], G. Batignani[13,14], J. Baudot[6], P. K. Behera[9], S. Bettarini[13,14], T. Bilka[5], A. Bozek[22], F. Buchsteiner[2], G. Casarosa[13,14], Y. Q. Chen[4], L. Corona[13,14], T. Czank[18], S. B. Das[10], N. Dash[9], G. Dujany[6], F. Forti[13,14], M. Friedl[2], E. Ganiev[15,16], B. Gobbo[16], S. Halder[12], K. Hara[20,17], S. Hazra[12], T. Higuchi[18], C. Irmler[2], A. Ishikawa[20,17], H. B. Jeon[21], Y. Jin[16], C. Joo[18], M. Kaleta[22], A. B. Kaliyar[12], J. Kandra[5], K. H. Kang[21], P. Kapusta[22], P. Kodyš[5], T. Kohriki[20], M. Kumar[10], R. Kumar[11], P. Kvasnička[5], C. La Licata[18], K. Lalwani[10], S. C. Lee[21], Y. B. Li[3], J. Libby[9], S. N. Mayekar[12], G. B. Mohanty[12], T. Morii[18], K. R. Nakamura[20,17], Z. Natkaniec[22], Y. Onuki[19], W. Ostrowicz[22], A. Paladino[13,14], E. Paoloni[13,14], H. Park[21], G. Polat[7], K. K. Rao[12], I. Ripp-Baudot[6], N. Rout[9], D. Sahoo[12], C. Schwanda[2], J. Serrano[7], J. Suzuki[20], S. Tanaka[20,17], H. Tanigawa[19], R. Thalmeier[2], T. Tsuboyama[20,17], Y. Uematsu[19], O. Verbycka[22], L. Vitale[15,16], K. Wan[19], J. Webb[1], J. Wiechczynski[14], H. Yin[2], L. Zani[7]

(Belle-II SVD Collaboration)

[1]*School of Physics, University of Melbourne, Melbourne, Victoria 3010, Australia*
[2]*Institute of High Energy Physics, Austrian Academy of Sciences, 1050 Vienna, Austria*
[3]*Peking University, Department of Technical Physics, Beijing 100871, China*
[4]*University of Science and Technology of China, Department of Modern Physics, Hefei 230026, China*
[5]*Faculty of Mathematics and Physics, Charles University, 121 16 Prague, Czech Republic*
[6]*IPHC, UMR 7178, Université de Strasbourg, CNRS, 67037 Strasbourg, France*
[7]*Aix Marseille Université, CNRS/IN2P3, CPPM, 13288 Marseille, France*
[8]*Indian Institute of Technology Bhubaneswar, Satya Nagar, India*
[9]*Indian Institute of Technology Madras, Chennai 600036, India*
[10]*Malaviya National Institute of Technology Jaipur, Jaipur 302017, India*
[11]*Punjab Agricultural University, Ludhiana 141004, India*
[12]*Tata Institute of Fundamental Research, Mumbai 400005, India*
[13]*Dipartimento di Fisica, Università di Pisa, I-56127 Pisa, Italy*
[14]*INFN Sezione di Pisa, I-56127 Pisa, Italy*
[15]*Dipartimento di Fisica, Università di Trieste, I-34127 Trieste, Italy*
[16]*INFN Sezione di Trieste, I-34127 Trieste, Italy*
[17]*The Graduate University for Advanced Studies (SOKENDAI), Hayama 240-0193, Japan*
[18]*Kavli Institute for the Physics and Mathematics of the Universe (WPI), University of Tokyo, Kashiwa 277-8583, Japan*
[19]*Department of Physics, University of Tokyo, Tokyo 113-0033, Japan*
[20]*High Energy Accelerator Research Organization (KEK), Tsukuba 305-0801, Japan*
[21]*Department of Physics, Kyungpook National University, Daegu 41566, Korea*
[22]*H. Niewodniczanski Institute of Nuclear Physics, Krakow 31-342, Poland*

E-mail: giuliana.rizzo@pi.infn.it

(Received December 12, 2020)

In spring 2019 the Belle II experiment at the high-luminosity SuperKEKB e^+e^- collider (KEK, Japan) has resumed operation after the installation of the new vertex detector. In the first period of operation SuperKEKB has already reached the record luminosity of 2.4×10^{34} cm^{-2}s^{-1}, which will be increased by about a factor 30 in the coming years. Two inner layers of DEPFET-based pixels and four layers of double-sided silicon strip detectors (Silicon Vertex Detector, SVD) make up this new vertex detector, designed to meet the stringent physics requirements as well as to cope with the high beam background conditions. Since the beginning of data taking, the SVD has been functioning with a very reliable and stable operation and excellent detector performance. The first evidence of radiation effects in the SVD have been observed, which are at the expected level and not affecting performance. This paper will review the performance achieved by the SVD and the lessons learned in the first year of operation that continued even during the COVID-19 pandemic.

KEYWORDS: Silicon strip detector, Vertex detector, Tracking detector, Belle II

1. Introduction

The Belle II experiment [1], operating at the SuperKEKB asymmetric-energy e^+e^- collider (KEK, Japan) [2], will play a crucial role in the next years in the search for new physics beyond the Standard Model. SuperKEKB is the upgraded KEK B-Factory, with a center-of-mass energy of 10.58 GeV corresponding to the peak of the $\Upsilon(4S)$ resonance. It has been designed to reach an unprecedented instantaneous luminosity of 8×10^{35} cm^{-2}s^{-1}, although recent studies indicated that going behind 6×10^{35} cm^{-2}s^{-1} might be very difficult. An integrated luminosity of 50 ab^{-1} is achievable with the new machine in a few years of operation.

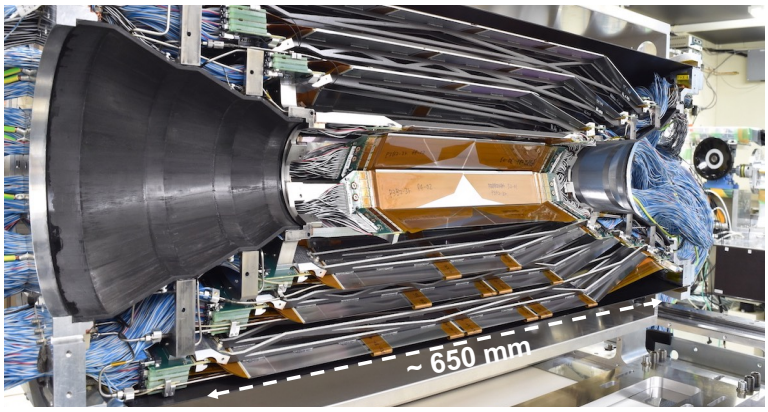

Fig. 1. Picture of half of the SVD before the insertion into the Belle II detector.

To fully exploit the rich physics program accessible with this luminosity upgrade, the Belle detector has also been partially upgraded to meet the more stringent physics requirements and to cope with the higher beam background expected with the new high-luminosity machine. In particular, Belle II has now a new vertex detector (VXD) designed to ensure a precise reconstruction of decay vertices of B and D mesons, as well as of unstable particles that decay close to the interaction point (IP), and to perform low-momentum particle tracking in the new high-background environment. The VXD is composed of the Pixel Detector (PXD), with two inner layers of DEPFET-based pixels, and the Silicon Vertex Detector (SVD) made of four layers of double-sided silicon strip detectors. After the installation of the VXD, in spring 2019, the Belle II experiment has started its first physics run with the complete detector.

This paper will review the main features of the SVD, its operational experience and the performance achieved in the first year of data taking, together with the initial effects of radiation damage.

2. SVD Overview

The SVD is composed of four layers of ladders assembled with double-sided silicon strip detectors (DSSD) and read-out with the APV25 front-end chips [3]. The SVD layers 3, 4, 5 and 6, are located respectively at radii of 39 mm, 80 mm, 104 mm and 135 mm, covering a polar angle region $17° < \theta < 150°$ and the full azimuth with respect to the e^- beam.

A picture of one half of the SVD before its insertion in Belle II is shown in figure 1. A longitudinal schematic view of the SVD is shown in figure 2 with a picture of a layer 6 ladder including an exploded view of its various components.

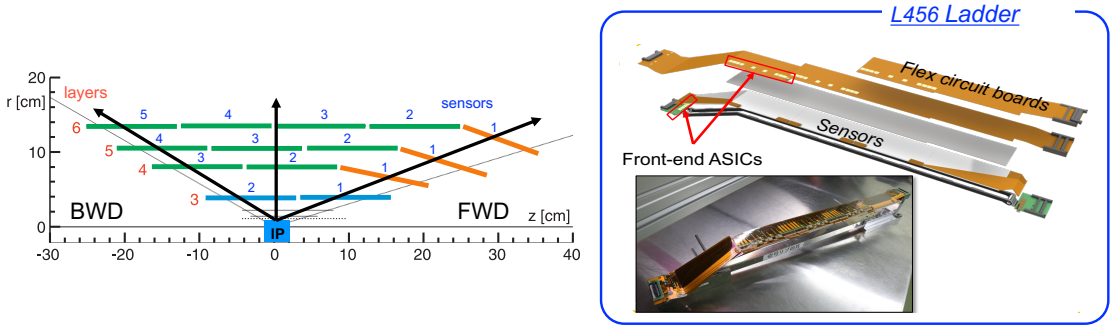

Fig. 2. Schematic of the SVD layout (left). Picture of a layer 6 ladder with an exploded view of its various components (right).

The main feature of the three types of SVD silicon sensors are listed in table I. Two small rectangular sensors are used for short ladders in layer 3, with a simple barrel shape. Ladders of layers 4, 5 and 6 are composed of two to four large rectangular sensors with a slanted trapezoidal sensor used in the forward region to minimize the material and instrumented surface, while still covering the largest polar angle, giving the detector a lantern-like shape. The total silicon area is about 1.2 m^2.

For efficient background suppression, the fast APV25 read-out chip is adopted, which has 50 ns peaking time and matches well the capacitive load of the strips to provide a good signal-to-noise ratio for all the layers.

Table I. Details of the double-sided silicon strip sensor types used in the SVD. All sensors have one intermediate floating strip between two readout strips. The local coordinates (u,v) measure the positions on the p and n-sides, respectively.

	Small Sensors	Large Sensors	Trapezoidal Sensors
Number of readout strips (u/p-side - $r-\phi$)	768	768	768
Number of readout strips (v/n-side - z)	768	512	512
Readout pitch (u/p-side - $r-\phi$)	50 μm	75 μm	75-50 μm
Readout pitch(v/n-side - z)	160 μm	240 μm	240 μm
Sensor active area (mm^2)	122.90 x 38.55	122.90 x 57.72	122.76 x (57.59-38.42)
Sensor thickness	320 μm	320 μm	300 μm
Manufacturer	Hamamatsu	Hamamatsu	Micron

In the layers 4, 5 and 6 the central DSSDs are individually read out by a novel Origami chip-on-sensor concept. In this scheme APV25 chips thinned down to 100 μm are placed on flexible circuits, which are glued on top of the sensors. Thanks to flexible pitch adapters, which are wrapped around the edge of the sensors, the strips of both sides of the DSSDs are read out from the top. This Origami chip-on sensor design has two main benefits. It allows to connect each sensor individually to the APV25 chips, minimizing the analog path length and reducing capacitive noise. In addition, with all the readout chips placed on the same side of the DSSD sensors, material for the cooling can be minimized using the same cooling pipe for all of them. Further details on the construction of the SVD ladders can be found in [4]. By optimizing the ladder design and support structures, as well as using an evaporative CO_2 cooling system, an average material budget per ladder of 0.7% of a radiation length has been achieved.

3. Operational Experience

The operation of SVD has been smooth and reliable since the beginning of the data taking in spring 2019, with very good performance, which is presented in section 4.

The calibration constants, such as pedestal, noise and the gain, used for the online zero suppression and for the offline reconstruction, are frequently monitored to ensure efficient operation. They are extremely stable in time, except for some expected increase in noise due to radiation damage as shown in section 5. The number of bad APV25 channels (i.e. with anomalous values of the calibration constants) is at the level of 1% and stable in time. These bad channels are mainly due to defective strips on the sensors, which were already identified during sensor testing and ladder construction.

In the first few months of data taking, until July 2019, only one APV25 chip in a layer 3 ladder (out of 1748 chips in the SVD) has been disabled owing to a connection problem that deteriorated with time. This problem has been fixed during the summer 2019 shutdown, when it was possible to access and reconnect the module cable close to the VXD area.

The CO_2 cooling plant, operated at -20°C, is working well and the detector temperature has been very stable, ranging from 5° to 30°C, as monitored by sensors located in different VXD areas. Since the layer 3 is very close to PXD, temperature variations of about 2-3°C, and corresponding changes in the sensor leakage current, are observed when PXD changes its power consumption, due to different power settings applied. However, such variations do not affect the performance.

During the first year of operation a couple of effects required attention, although they did not affect the detector performance.

The first one is that the trapezoidal Micron sensors show a turn-on effect: noise on the n-side of the sensors and the leakage current take up to a few hours to reach steady conditions after the bias voltage is turned on. After steady conditions are reached, they are retained even if the bias voltage is turned off for less than one hour, as during refill of the machine after beam aborts. This effect, also observed in ATLAS semiconductor tracker strip sensors [5], is probably due to some slow drift of charges on the sensor surface in the very dry environment, which is then changing the extension of the electron accumulation layer present on the n-side of the sensor. This variation affects the interstrip capacitance and consequently the noise on the n-side, and it also changes the extension of the area that contributes to the leakage current generated at the n-side surface. The only operational impact of this effect, at the level of 10% in noise variation, is the necessity to take the calibration run for noise measurements, used for the online zero suppression, only when the steady conditions are reached.

The second effect is that one sensor in layer 6 developed a high leakage current when SuperKEKB started operating with continuous injection. A similar effect was also observed in the past in some BaBar Silicon Vertex Tracker (SVT) sensors [6]. All the observations and tests performed are compatible with the following interpretation: positive charge, due to radiation-induced ionization of the air in the region between the sensors, can accumulate on the p-side sensor surface (junction side), in-

creasing the local electric field. Charge accumulation is driven by the high electric field in air present between the layer 5 n-side, with positive bias, and the layer 6 p-side, with negative bias, as shown schematically in figure 3. The increase in leakage current is due to generation from impact ionization, caused by the local increase of the sensor electric field on the p-side, concomitant with a pre-existing sensor defect in that location.

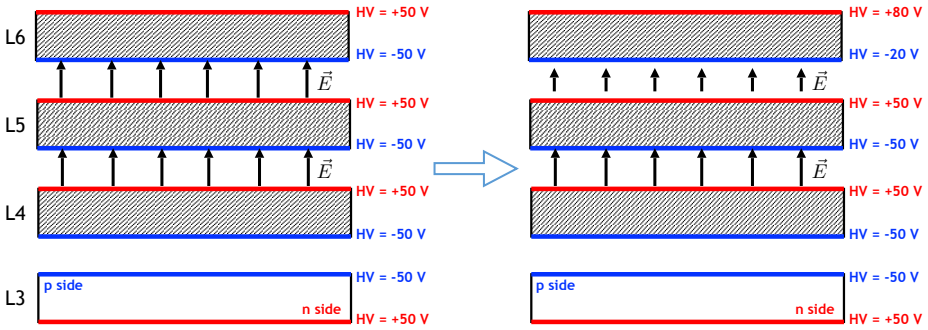

Fig. 3. Schematic view of the bias voltage configuration (HV) between the four layer of the SVD. On the left the original setting and on the right the new setting with the shift applied to reduce the electric field in air present between layer 5 n-side and the layer 6 p-side, still keeping the full bias voltage of 100V.

The countermeasure adopted in June 2019, when the sensor had already reached a total current of about 40 μA, was to shift the bias voltage settings between layer 5 and layer 6, reducing the electric field in air, but still keeping the full bias voltage of 100V in each sensor. This bias voltage shift is effective in keeping the detector leakage current under control. No degradation of the sensor performance has been observed and the leakage current is likely concentrated in a few strips that are showing higher noise while the leakage is high. No other sensors have developed similar symptoms.

During the COVID-19 pandemic emergency Belle II continued data taking throughout 2020, re-organizing the operation with more coverage from remote shifters. Accordingly the organization of the SVD operation was changed, relying on an SVD operation coordinator, resident at KEK, assisted by a 24/7 coverage provided by remote shifters for the standard remote operation and data quality monitoring. A smooth data taking, even with the COVID-19 travel restrictions, was possible thanks to the dedication of the few SVD colleagues based at KEK, that were following the SVD operation and were readily available for any hardware interventions.

4. Performance

In the first one and a half years of data taking with the SVD installed, up to July 2020, Belle II has recorded approximately 70 fb^{-1} integrated luminosity at the $\Upsilon(4S)$ peak. These first data confirmed an excellent performance of all the 172 SVD sensors, with stable behaviour over time. The main results achieved for cluster charge and signal-to-noise ratio, hit efficiency, as well as position and time resolution are summarized in this section.

The signal produced by particles traversing the SVD strongly depends on the track incident angle with respect to the sensor's surface, which defines the path length in silicon. Sensors at different z positions along the ladders are traversed by tracks coming from the IP with different angles, as schematically shown in figure 2. This is reflected well in the reconstructed cluster charge distribution for the various sensors. An example of the cluster charge, for clusters associated with tracks, is shown in the top-row plots in figure 4, for two sensors in different z positions along the layer 4 ladders.

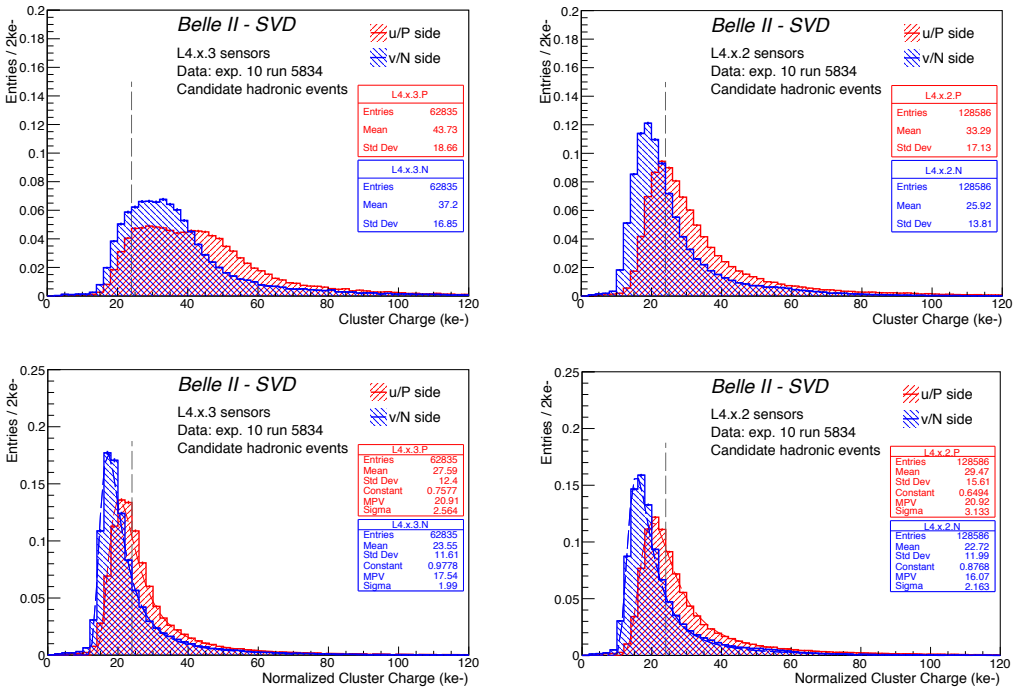

Fig. 4. Cluster charge (top row) and cluster charge normalized to track length (bottom row) for sensors in specific z positions in layer 4, summed over all ϕ ladders. Backward sensors (L4.x.3) on the left and central sensors (L4.x.2) on the right. The vertical dashed lines correspond to the MIP signal.

The correct calibration of the system is verified evaluating the cluster charge normalized to the track length, shown in the bottom-row plots in figure 4 for the same sensors. The distribution of the normalized cluster charge is similar for all sensor positions and has the expected Landau shape with a most probable value (MPV) of about 21 ke^- on the u/p-side, for the 320 μm thick sensors. This measured value is in fair agreement with the expected signal for a MIP (24 ke^- in 320 μm silicon), taking into account an uncertainty of about 15% on the preliminary absolute APV25 gain calibration used in these data. The internal calibration circuit of the APV25 allows to measure the relative gain of each channel, that has a large spread among different chips [7]. For the absolute gain calibration (i.e. the conversion of the pulse injected in the calibration circuit to input signal in electrons) preliminary values extracted from testbeam data are used. These are based on only a few chips on prototype ladders, so the large spread of about 15% in the relative gain among different chips is still affecting this absolute gain calibration and it will be improved in future, using data from the entire detector.

In figure 4 there is a 10%-25% reduction of the charge on the v/n-side with respect to the signal on the u/p-side, explained by the charge loss due to the presence of the floating strip combined with the large pitch on the n-side. A good energy calibration is important for particle identification exploiting the energy-loss information in the SVD, particularly beneficial for low momentum particles [8].

The signal-to-noise ratio (SNR) for clusters on tracks is an important figure of merit to be monitored. Defined as the total cluster charge over the quadrature sum of the noise of each strip belonging to the cluster, it depends on the collected charge and strip noise, as well as on the cluster size. Both the cluster signal and the cluster size depend strongly on the incident angle, and therefore on the sensor position. The noise in the u/p-side with longer strips and smaller pitch is higher than that in the v/n-side, up to a factor two: the equivalent noise charge (ENC) is 750–1000 e^- on u/p-side and 500–650 e^- on v/n-side. The SNR is therefore in general higher on the v/n-side, with quite large

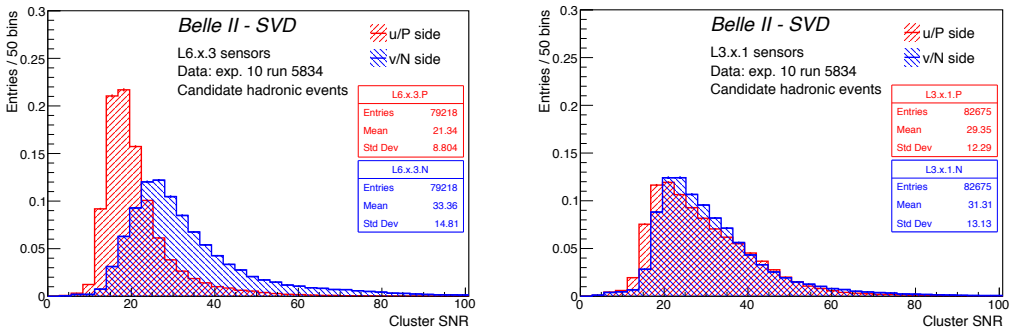

Fig. 5. Signal-to-noise ratio for sensors in specific z position, summed over all ϕ ladders . Third sensor in layer 6 (L6.x.3) on the left and forward sensor in layer 3 (L3.x.1) on the right.

variation among the various sensors, depending on their position. The measured MPV SNR value is very good in all 172 sensors, ranging between 13 and 33 depending on the sensor position and side; a few examples are shown in figure 5.

An excellent and very stable hit efficiency has been observed for all sensors. The hit efficiency is measured extrapolating the reconstructed tracks on the sensor surface and counting how often a cluster is found within 0.5 mm from that intercept on the sensor. On average it is above 99.5%, with the majority exceeding 99%; the few exceptions, with about 98%, are due to a higher than average number of defects that were already observed during module assembly. The stability of the hit efficiency is monitored with data quality plots that are constantly checked during data taking to assess the quality of each run, together with other significant SVD variables used for this evaluation.

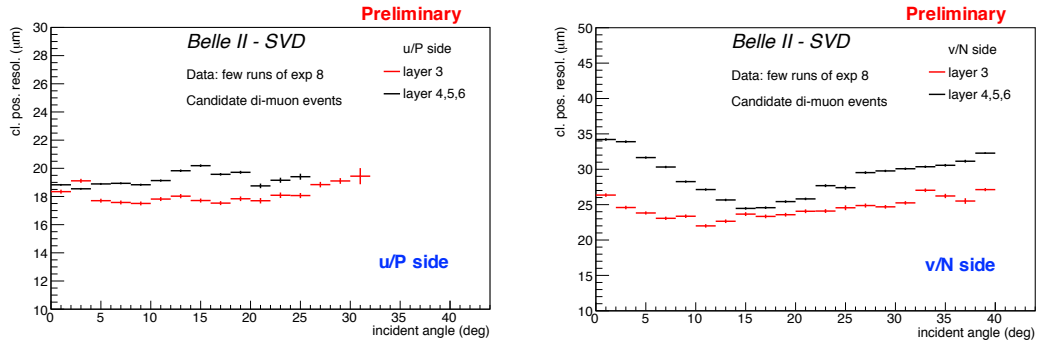

Fig. 6. Cluster position resolution as a function of the track incident angle projected on the plane orthogonal to the strips for the u/p (left) and v/n-side (right) for layer 3 and outer layer sensors.

The position resolution is estimated, with di-muon events, by using the residuals of the cluster position with respect to the track extrapolation, subtracting the effect of the track extrapolation uncertainty. The measured resolution as a function of the track incident angle projected on the plane orthogonal to the strips is shown in figure 6. Results on the v/n-side, between 25-35 μm, are in reasonable agreement with the expectation, while the values on the u/p-side, 18-20 μm, are larger than foreseen for the given small pitch, although they are adequate with respect to the required performance. Additional studies are now ongoing to optimize the reconstruction algorithms on data to further improve position resolution. Also, the simulation is now being tuned to improve the agree-

ment with data, especially in cluster size, that was underestimated causing a too optimistic position resolution in MC events. Good progress has been recently achieved by simulating the charge sharing coupling coefficients measured directly on data.

The very fast response of the APV25 allows a precise measurement of the cluster time, useful for an efficient rejection of beam background hits, off-time with respect to the triggered event. The APV25 output shaper response is sampled every 31 ns, with 6 samples readout for each strip. As explained in detail in reference [9] the strip time is measured as the calibrated centre-of-gravity of the samples provided by the APV25 and the cluster time is the weighted average of the strip time with the strip charge. With this method a very good cluster time resolution of about 2.5 ns has been achieved, that will be crucial for background rejection to maintain excellent tracking performance even in future operation with higher beam background.

5. Beam Background and Radiation Damage

In the beginning of Belle II operation, with relatively small beam currents and luminosity, machine related background and radiation levels in the SVD have been relatively low during data taking. This initial phase is crucial to perform detailed background studies with different beam currents and machine conditions, comparing them with the corresponding MC expectations. These early data provide an absolute scale for the background extrapolations to design luminosity [10], which, while still affected by large uncertainties, have become significantly more reliable than the initial estimates.

Although modest and not affecting performance, the effects of the radiation damage are visible since the first months of operation with beams and they are monitored to compare them with the expectations.

In the 2019 and 2020 physics runs the strip occupancy in the layer 3 sensors has been at the level of 0.3%. Current background extrapolations indicate that this occupancy could reach about 3-5% at design luminosity, although these estimates have still a large uncertainty. Further mitigation strategies are under study on the machine side to reduce the background levels. With the current algorithms, tracking performance starts to gradually deteriorate at about 3% occupancy, but preliminary results exploiting background rejection based on hit time selection, not yet deployed in reconstruction, indicate that this limit can be significantly increased. In this perspective, the SVD occupancy should allow good tracking performance even at design luminosity, although it could be close to the limit.

There is a higher safety margin for the effects related to radiation damage caused by total ionizing dose (TID) and non-ionizing energy loss (NIEL), relevant for the SVD lifetime. Simulations of the SVD background radiation field indicate that a 1 MeV equivalent neutron fluence of 1.5×10^{11} n_{eq}/cm^2 corresponds to about 100 krad for the SVD Layer 3 sensors. Estimated SVD silicon sensors leakage current increase and depletion voltage shift are not expected to cause any significant performance deterioration up to 10 Mrad and 1.5×10^{13} n_{eq}/cm^2 equivalent neutron fluence. APV25 chips have been qualified to operate up to 100 Mrad.

The background extrapolation at design luminosity gives an estimate of 0.3-0.5 Mrad/yr on average in Layer 3 sensors, and an equivalent neutron fluence of $4.5\text{-}7.5\times10^{11}$ n_{eq}/cm^2. This estimate does not include the injection background nor the additional dose delivered during machine tuning operation, but a reasonable margin is left even after a few years of operation at design luminosity.

Diamond sensors are installed in several locations around the interaction region and are used both as a radiation monitor and in the beam abort system [11]. The integrated radiation dose in the SVD sensors is estimated from the diamond sensors exploiting the correlation of the SVD occupancy with the instantaneous dose rate measured by the diamonds detectors located on the beam pipe. The method relies on several assumptions and the uncertainty in the estimated dose is high, up to a factor two, still this rough estimate is very useful to correlate the effect of radiation damage observed with the expectations.

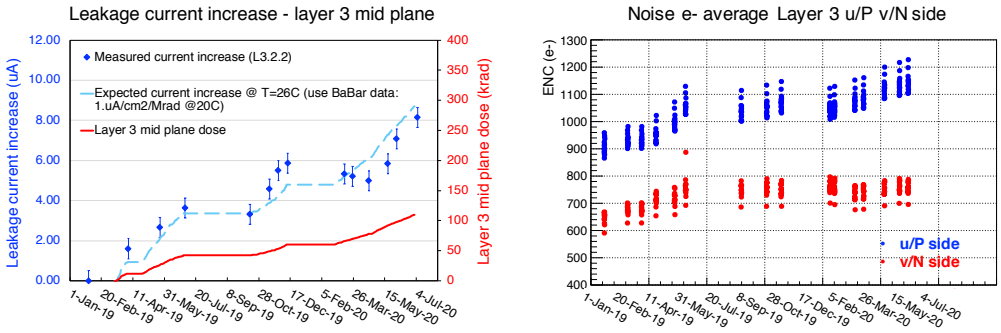

Fig. 7. Comparison between the expected and measured leakage current increase as a function of time and the corresponding total integrated dose estimated from diamonds for one of the layer 3 sensors in the mid plane (left). Noise evolution with time of layer 3 sensors, between January 2019, before starting operation, and July 2020 (right).

The integrated dose as a function of time in the most exposed sensors in the layer 3 mid plane is shown in the left plot of figure 7. As of July 2020, about 100 krad is integrated in these sensors, while the average dose in all layer 3 sensors is about 70 krad, and ranges from 10 to 20 krad for the other layers.

This relatively high dose is dominated by high background conditions during vacuum scrubbing or machine optics and collimator tuning, particularly frequent during the first 1.5 years of operation. Therefore, it cannot be directly compared with the Layer 3 average dose of 0.3-0.5 Mrad/yr expected at design luminosity, which only takes into account stable beam operation.

The increase in sensor leakage current due to radiation damage is clearly visible since the first months of beam operation. As an example the leakage current increase as a function of time for one of the layer 3 sensors in the mid plane is shown in the left plot of figure 7 compared with the expected increase estimated using BaBar SVT sensor data, about 1 μA/Mrad/cm^2 at 20°C, re-normalized to 26°C for Layer 3 sensors. Since the radiation fields in BaBar and Belle II vertex detectors are expected to be similar, data from BaBar sensors are considered to be a good estimate of the effect we can expect in the SVD. The leakage current increase measured in the BaBar sensors was confirmed to be mainly due to bulk damage from low energy electrons [6] with dedicated irradiation campaigns.

Given current data, even after 10 Mrad the leakage current increase is not expected to significantly affect the noise figure. With the fast 50 ns APV25 shaping time the noise is in fact dominated by the sensor capacitance, whose contribution to the equivalent noise charge squared is inversely proportional to the shaping time, while the shot noise term, coming from the leakage current and proportional to the shaping time, is negligible.

The noise evolution as a function of time for layer 3 sensors is shown in the right plot of figure 7. A noise increase up to 15% and 25% has been observed on v/n and u/p-sides, respectively, up to July 2020. In the outer layers, exposed to lower dose, the increase of noise levels has been only around 5–10%. The observed effect is not related to the increase in sensor leakage current, which is not dominant as explained above, and it is instead likely due to some initial effect of radiation damage to the sensor surface. The higher fixed oxide charge induced by radiation increases the interstrip capacitance and therefore the strip noise. The noise increase has already shown some saturation effect on the v/n-side of the sensors and it is expected to saturate also in the u/p-side, since the increase in the fixed oxide charge will also saturate.

We have developed an effective and relatively fast method to monitor possible future changes in depletion voltage due to bulk damage. The depletion voltage for the installed sensors is evaluated with

a simple set of calibrations that measure the noise as a function of the bias voltage applied, without any need to use beam time for this measurement, as in other techniques based on the reconstruction of the clusters with different bias voltage. In our $p^+/n/n^+$ double-sided sensors, the depletion region expands from the p-side and the n-side strips are insulated only when the n-type bulk is fully depleted. When insulated, the noise on the n-side strips drops to a minimum level, indicating that the full depletion voltage is reached. With over-depletion the n-side noise continues slightly to decrease. The interstrip capacitance, that dominates the noise, is proportional to the ratio of the strip implants width over the pitch. On n-type bulk sensors the effective width of the n-strip implant is extended by the electron accumulation layer present on the n-side surface. Since over-depletion reduces the electron accumulation layer the noise is also reduced.

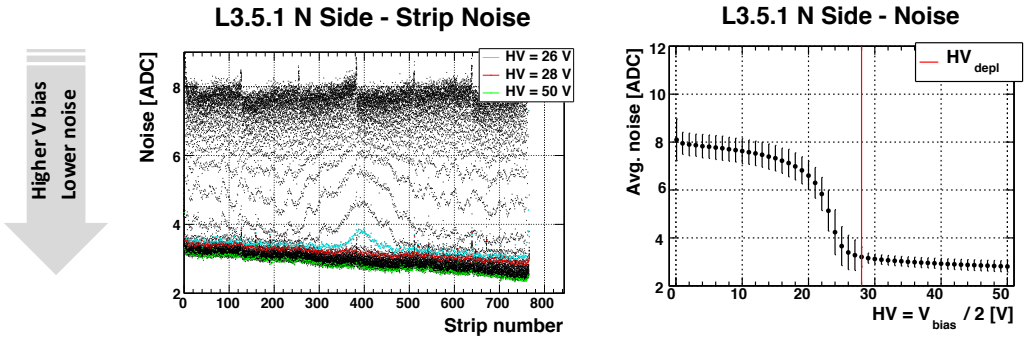

Fig. 8. Example of the noise in a layer 3 sensor during the July 2020 HV scan, used to measure the depletion voltage. The indicated HV is half of the bias voltage. On the left, the n-side strip noise as a function of the strip number for increasing HV. The red points corresponds to full depletion. On the right the average n-side noise vs. HV applied, with the red vertical line indicating the drop at V_{depl}= 56V (HV_{depl}=28V).

The method has been proven to work, with initial scans taken in the spring/summer 2020, when still no changes in depletion were expected given the low integrated fluence of about 1.5×10^{11} n_{eq}/cm^2. Results obtained are in good agreement, within a couple of volts, with the depletion voltage measured directly on the sensor before their assembly. An example of the behaviour of the n-side strip noise as a function of the bias voltage is shown in figure 8 for a layer 3 sensor, showing a depletion voltage of 56 V. All the 172 installed sensors have an initial depletion voltage between 20 and 60 V.

6. Conclusions & Outlook

The new Silicon Vertex Detector has started operation during physics run in the Belle II experiment from spring 2019. Since the beginning of data taking it has shown a very reliable and stable operation with excellent performance. Signal-to-noise ratios between 13 and 33, as well as average hit efficiency above 99.5%, have been measured with first data. A good spatial resolution of 18–35 μm has been obtained and studies are ongoing to further optimize the reconstruction algorithms as well as to tune the simulation for a better agreement with data. A very good hit time resolution of about 2.5 ns has also been achieved, which will be crucial during the future operation with higher beam-related background with the increased luminosity. First evidence of radiation effects in the SVD have been observed, which are at the expected level and are not affecting performance.

7. Acknowledgment

This project has received funding from the European Union's Horizon 2020 research and innovation programme under the Marie Sklodowska-Curie grant agreements No 644294 and 822070. This work is supported by MEXT, WPI, and JSPS (Japan); ARC (Australia); BMWFW (Austria); MSMT (Czechia); CNRS/IN2P3 (France); AIDA-2020 (Germany); DAE and DST (India); INFN (Italy); NRF-2016K1A3A7A09005605 and RSRI (Korea); and MNiSW (Poland).

References

[1] T. Abe et al., "Belle II Technical Design Report", (2010), arXiv:1011.0352.
[2] Y. Ohnishi et al., "Accelerator Design of SuperKEKB", Prog. Theor. Exp.Phys **2013**, 03A011 (2013).
[3] M.J. French et al., "Design and results from the APV25, a deep sub-micron CMOS front-end chip for the CMS tracker", Nucl. Instrum. Meth. A **466**, 2 (2001).
[4] K. Adamczyk et al., "The Belle II silicon vertex detector assembly and mechanics", Nucl. Instrum. Meth. A, **845** 38 (2017).
[5] A. Chilingarov et al., "Interstrip capacitance stabilization at low humidity", Nucl. Instrum. Meth. A, **560** 118 (2006).
[6] B. Aubert et al., "The BABAR Detector: Upgrades, Operation and Performance", Nucl. Instrum. Meth. A **729**, 615 (2013).
[7] M. Raymond et al.,"Final Results from the APV25 Production Wafer Testing", 11th Workshop on Electronics for LHC and Future Experiments (LECC 2005) 91 (2005).
[8] S. Hazra et al.,"Particle Identification in Belle II Silicon Vertex Detector", these JPS Conf. Proc.
[9] Y. Uematsu et al.,"A Study for Hit-time Reconstruction of Belle II Silicon Vertex Detector", these JPS Conf. Proc.
[10] H. Tanigawa et al., "Beam background study for the Belle II Silicon Vertex Detector", Nucl. Instrum. Meth. A **982** 164580 (2020).
[11] S. Bacher et al.,"Performance of the diamond-based beam-loss monitor system of Belle II", submitted to Nucl. Instrum. Meth. A.